Research on eco-hydro-morphological river processes by combining field investigations, physical modeling and numerical simulations

K. Blanckaert[1,2,3,4], W. van Balen[3,5], A. Duarte[2], V. Dugué[2], X.-F. Garcia[4], , W. Ottevanger[3], M.T. Pusch[4] A. Ricardo[2], I. Schauder[4], A. Sukhodolov[4], W.S.J. Uijttewaal[3], R. Wilkes[4]

[1] *State Key Laboratory of Urban and Regional Ecology, Research Center for Eco-Environmental Sciences (RCEES), Chinese Academy of Sciences (CAS), Beijing, China*
[2] *Laboratory of Hydraulic Constructions (LCH-ENAC), Ecole Polytechnique Fédérale Lausanne (EPFL), CH-1015 Lausanne, Switzerland.*
[3] *Faculty of Civil Engineering and Geosciences, Delft University of Technology, Delft, The Netherlands.*
[4] *Department of Ecohydrology, Institute of Freshwater Ecology and Inland Fisheries, Berlin, Germany*
[5] *HKV Consultants, Postbus 2120, 8203 AC Lelystad, The Netherlands*

koen.blanckaert@epfl.ch

Abstract
Hydrodynamical, morphodynamical and ecological river processes and their multiple linkages occur in an infinity of different configurations and over a wide range of spatial and temporal scales. This paper illustrates a research methodology that consists in combining field investigations, physical modeling in the laboratory, and numerical simulations in order to develop generic insight and tools for engineering and management of the river environment. This combined methodology is illustrated in research on (i) the macroscale characteristics of the velocity distribution and their relation to long-term and large-scale planimetric river processes, (ii) the flow field in the vicinity of the river bank and its importance with respect to bank erosion and, (iii) linkages between the characteristics of the mean flow and the turbulence on the one hand, and the behavior of invertebrates on the other. The reported research strongly relies on the use of state-of-the-art measuring instruments as well as numerical techniques.

Keywords: *field investigation, physical model, numerical simulation, meander, hydrodynamics, morphology, ecohydraulics*

1. Introduction

Hydrodynamical, morphodynamical and ecological river processes and their multiple linkages occur in an infinity of different configurations and over a wide range of spatial and temporal scales. This complicates the development of generic insight and tools for engineering and management of the river environment.

The present paper illustrates a research methodology that consists in combining field investigations, physical modeling in the laboratory, and numerical simulations. Field investigations allow identifying and observing the processes of relevance in the natural environment. But their analysis and interpretation is complicated by the lack of control on the natural river environment and by interferences between all simultaneously occurring processes. Laboratory experiments in simplified schematized configurations allow isolating and/or accentuating certain processes under controlled condition. Moreover, they allow investigating the dependence of these processes on the control parameters as well as defining guidelines and requirements for the numerical modeling of these processes. Field investigations and laboratory experiments are inherently limited to a small number of configurations. Numerical models allow broadening the parameter space. But they are only reliable after validation by means of the experimental data provided by the field and laboratory investigations.

The objective of the present paper is to illustrate the application of this combined methodology to investigate processes occurring on different temporal and spatial scales. Section 3 focuses on the macroscale characteristics of the velocity distribution and their relation to long-term and large-scale planimetric river processes. Section 4 highlights the flow field in the vicinity of the river bank and its importance with respect to bank erosion. Section 5 reports research on linkages between the characteristics of the mean flow and the turbulence on the one hand, and the behavior of invertebrates on the other. The reported research strongly relies on the use of state-of-the-art measuring instruments (section 2) as well as numerical techniques (sections 3, 4).

2. Measuring instruments

Enhancing the understanding of hydrodynamical, morphodynamical and ecological river processes and their linkages requires accurate knowledge of the three-dimensional flow field as well as the large turbulent structures.

The laboratory experiments reported in this paper made use of an Acoustic Doppler Velocity Profiler (ADVP, see Figure 1) developed at Ecole Polytechnique Fédérale Lausanne (EPFL, Switzerland). The ADVP's working principle and estimates of the accuracy in the measurements have been reported by Lemmin and Rolland ([1]), Hurther and Lemmin ([2]), Blanckaert and Graf ([3]), Blanckaert and de Vriend ([4]), Blanckaert and Lemmin ([5]). Blanckaert ([6]) discusses the methodological advantages of the ADVP over commercially available velocimeters. The ADVP measures profiles of the three-dimensional velocity vector $\vec{v}(t) = (v_s, v_n, v_z)(t)$. The velocity vector is decomposed in an orthogonal reference system with curvilinear streamwise *s*-axis along the river centerline, transverse *n*-axis pointing towards the left bank, and vertically upward *z*-axis. The velocity range to be measured imposes a lower bound on the measuring frequency, whereas the maximum flow depth imposes an upper bound to the measuring frequency ([1]). The measuring frequency typically adopted in the laboratory experiments is about 30 Hz, which is sufficient to resolve the large scale turbulent structures. The profiling capacity of the ADVP enables measurements at high spatial resolution and resolving turbulent coherent structures.

Figure 1: Acoustic Doppler Velocity Profiler (ADVP) in the laboratory experiments. The horizontal size is about 25 cm.

The upper limit on the measuring frequency imposed by the flow depth does not allow resolving the large scale turbulence structures in field configuration with flow depths larger than about 1m by means of acoustic velocity profilers. Therefore, Nortek Acoustic Doppler Velocimeters (ADV) that measure the three-dimensional velocity vector with high temporal resolution in one single point were applied in the field investigations. In order to perform measurements with high spatial resolution, simultaneous measurements were made with an array of ADV's mounted on a bridge (Figure 2).

Figure 2: Array of Nortek Acoustic Doppler Velocimeters (ADV) in the field investigations.

3. The velocity distribution and its relation to long-term and large-scale river planform processes

Planform river processes occur on geological time scales and large spatial scales. This section focuses on the migration of meandering rivers, as illustrated in Figure 3. Meander migration occurs through erosion of the outer bank and corresponding accretion at the opposite inner bank.

Figure 3: Illustration of the migration of meandering rivers (picture from internet).

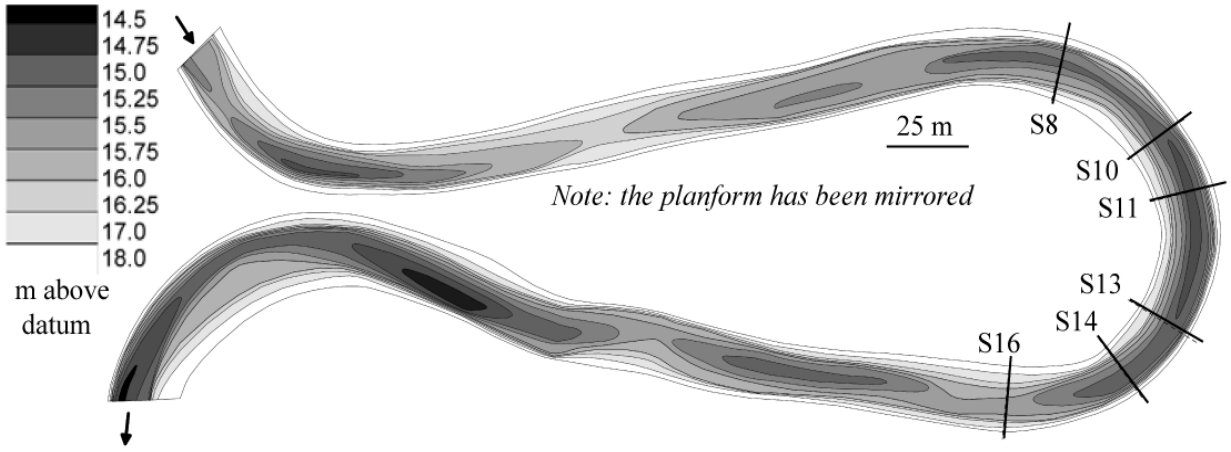

Figure 4. Planform and bathymetry of the meandering Ledra River (Courtesy A. Sukhodolov).

Field observations ([7]) indicate that the meander migration is largely driven by the hydrodynamics and can be modeled as:

$$M \sim \Delta U_s \tag{1}$$

Here M is the rate of erosion at the (concave) outer bank, which is equal to the accretion rate at the (convex) inner bank because the width does not significantly change in the process of meander migration. ΔU_s is the excess of velocity at the outer bank with respect to the average velocity in the cross-section, for conditions corresponding to the bankfull discharge. Hence the knowledge of the velocity field on the spatial scale of a single meander bend for one specific flow condition can enhance the understanding of long-term and large-scale meander migration.

A field investigation was performed on a bend on the Ledra River (Figures 4 and 5). IGB conceived the experimental set-up and provided the instruments and logistics of this field campaign that was coordinated by A. Sukhodolov. Flow depth and discharge varied by less than 5% during the measuring campaign, allowing for field measurements with an unprecedented spatial resolution on grids with more than 500 measuring points per cross-section. Six cross-sections were measured in detail in the bend illustrated in Figures 4 and 5. The investigated reach has a nearly constant width of about 15m, an overall-averaged water depth of about 1.5m, and a discharge of about 18 m^3s^{-1}. Flow is subcritical, Fr ≈ 0.3. The river is relatively narrow with an aspect ratio of about 10 and rather strongly curved with a ratio R_{max}/B = 3, where R_{max} is the centerline radius of curvature in the apex.

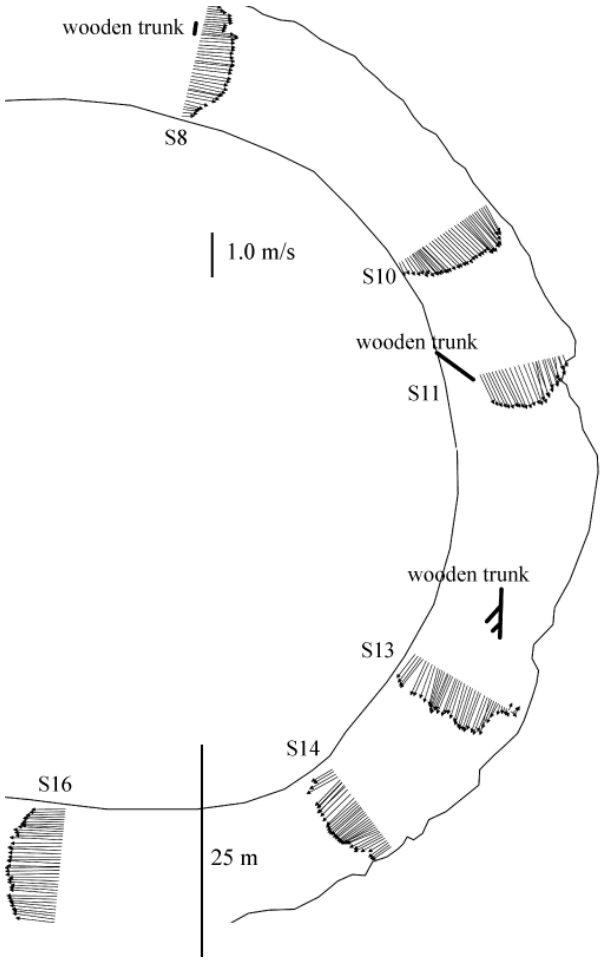

Figure 5: Depth-averaged velocity vectors (U_s,U_n) measured in the Ledra meander bend.

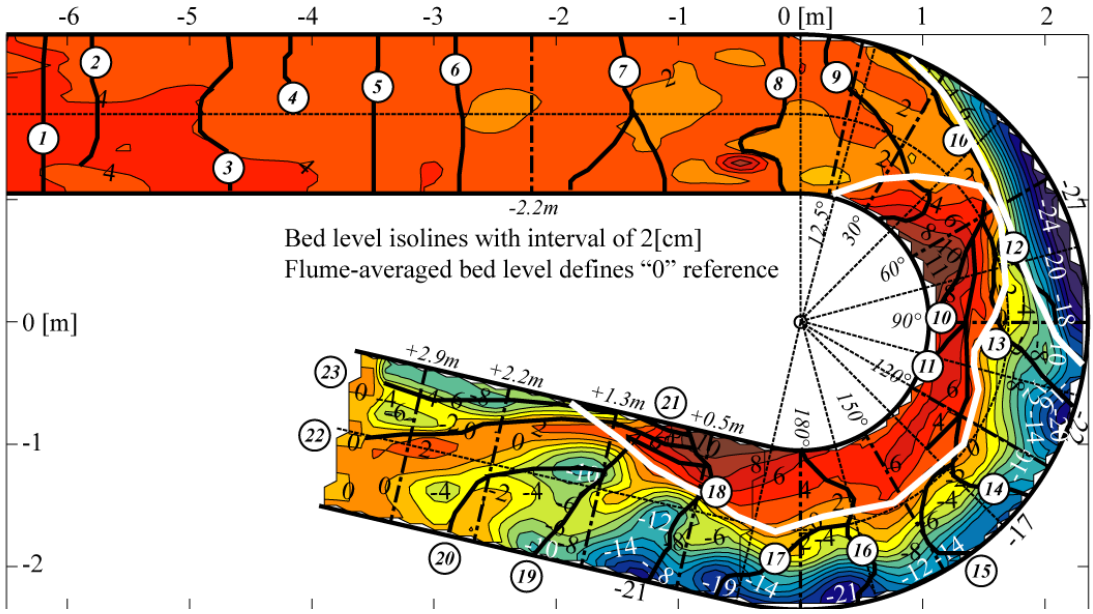

Figure 6. Isolines of the bed level with an interval of 0.02m derived from echosounder measurements. Additional ADVP measurement with higher spatial resolution are available in the indicated cross-sections. The position of dunes is based on photographs. The flume-averaged bed level defines the reference level. The white lines delineate approximatively the point bar and pool. (bottom).

Figure 6 illustrates the distribution of the depth-averaged velocity vectors (U_s,U_n), computed from measurements in about 30 vertical profiles with a vertical spacing of 0.1m between points. The velocity distribution is slightly inwards skewed in the cross-section S8 in the beginning of the bend, which may be attributed to the change in curvature. The velocity distribution is clearly outwards skewed in the cross-section S10, which requires outwards mass transport between S8 and S10. The maximum velocity excess at the outer bank clearly occurs in this cross-section S10 situated upstream of the bend apex. The core of maximum velocities has shifted inwards in cross-section S11. Surprisingly, the velocities are nearly uniformly distributed over the width in the second part of the bend. A slight outwards shift of the velocities occurs at the exit of the bend, which may be attributed to the decreasing curvature.

The analysis and interpretation of the velocity distribution in this meander bend are complicated by various factors typical of natural rivers. Wooden trunks that affect the hydrodynamics are present in the outer part of the bend upstream of cross-section S8, at the water surface in the inner part of the bend upstream of cross-section S11, and in the middle of the cross-section upstream of cross-section S13 (Figure 5). Moreover, vegetation, outer-bank benches and local bank erosion created an irregular geometry of the outer bank that considerably affects the flow.

Experiments in a physical laboratory model allow investigating the velocity distribution and the underlying processes under controlled conditions, without parasitical influences of wooden trunks, vegetation or irregular geometries. Moreover recent progress in instrumentation allows measuring the bed and water surface topographies (echosounders) and the 3D flow field (Acoustic Doppler Velocity Profiler) with unprecedented spatial and temporal resolution. Laboratory investigations concerning the bed topography have often been carried out with small flow depths ([8]), or under dynamic conditions with migrating bedforms ([9]) that did not allow for detailed velocity measurements whereas investigations of the flow field have often been carried out over schematized bed topographies ([10], [11]). Laboratory investigations including detailed measurements of the flow and the bed topography are extremely scarce ([12], [13], [14]).

The reported laboratory experiment was performed in the flume shown in Figure 6, which consists of a 193° bend of constant centerline radius of curvature, R = 1.7m, preceded by a 9m long straight inflow reach and a 5m long straight outflow reach. The width was constant at B = 1.3m. The bed consisted of mobile sand, with a mean diameter d = 2 mm. The flow and sediment discharges of Q=0.089 m^3s^{-1} and q_s = 0.023 $kgm^{-1}s^{-1}$, respectively, resulted in a flow field and a bed topography that were in equilibrium and representative of their counterparts in natural sharp meander bends. The flume averaged velocity and flow depth were U = 0.49 ms^{-1} and H = 0.141 m, respectively, yielding a Froude number of Fr = 0.41 The curvature ratio was R/B = 1.31 and the aspect ratio was B/H = 9.2.

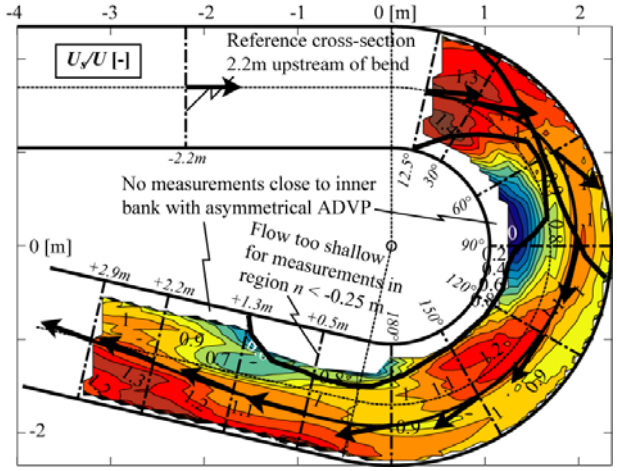

Figure 7: Normalized depth-averaged streamwise velocity, U_s/U [-]. Isoline pattern based on high-resolution measurements in the indicated cross-sections. The black lines delineate approximatively the point bar and pool. The black line with vectors indicates the first moment of the distribution of U_sh/UH, and the vectors $\left(\langle\langle U_s h\rangle\rangle, \langle\langle U_n h\rangle\rangle\right)/UH$.

Figure 7 shows the distribution around the flume of the normalized depth-averaged streamwise velocity. U_s/U. Moreover, it illustrates the location of the first moment (center of gravity) of the U_sh pattern as well as the vector $\left(\langle\langle U_s h\rangle\rangle, \langle\langle U_n h\rangle\rangle\right)$ ($\langle\langle\ \rangle\rangle$ represents cross-sectional averaged values). Similar to the Ledra bend, the maximum velocities are not systematically found over the deepest part of the cross-section. A potential vortex velocity distribution establishes just downstream of the bend entry with maximum values near the inner bank. The maximum velocities are subsequently found over the pool which requires strong outwards mass transport. The maximum value of $U_nh/UH \approx 0.7$ indicates that the flow seems to go straight on and to collide with the outer bank at an oblique angle at about 60° in the bend. A horizontal recirculation zone is observed over the shallow point bar, similar to recirculation zones observed in natural rivers ([15], [16], [17]). Flow does not separate at the bend entry, but only at about 40° in the bend, which can be attributed to the discontinuity in curvature at the bend entrance that leads to pronounced local accelerations/decelerations in the inner/outer-half of the cross-section and corresponding inwards mass transport that opposes flow separation. Therefore, this behavior is characteristic of zones of pronounced curvature increase. The flow recirculation zone reaches its maximum width in the cross-section at 80°, where it spans about 2/3 of the total width. The maximum velocities move again inwards downstream of the cross-section at 90°, accompanied by inwards mass transport. A pronounced outwards shift of the maximum velocity occurs at the bend exit, with corresponding strong flow deceleration over the shallow at the inside of the bend. Velocities tend to uniformise in the straight outflow reach. The pattern of depth-averaged streamwise velocities (Figure 7), leaves a clear footprint on the observed dune pattern (indicated in Figure 6), which is representative for the migration speed of the dunes and the related sediment transport rate. The overall features of the depth-averaged velocity pattern in the Ledra bend (Figure 5) and the laboratory bend (Figure 7) are quite similar. Gradients are more pronounced in the latter, however, which is due to the more pronounced curvature.

Blanckaert ([6]) has made a detailed analysis of the mechanism underlying the velocity redistribution by means of a term-by-term analysis of the depth-averaged momentum equation. This analysis revealed that the water surface gradient is the principal mechanism with respect to velocity (re)distribution. Inertia and curvature-induced secondary flow were also found to be processes of dominant order of magnitude, whereas turbulence was found to play only a minor role. The water surface gradient is mainly determined by the curvature and by changes in curvature. Curvature gives rise to a transverse tilting of the water surface (commonly called superelevation) which is inversely proportional to R. Hence, changes in the curvature throughout a bend lead to corresponding changes in the transverse water surface slope, and changes in the downstream water surface slope.

The dominant processes with respect to the velocity redistribution can be captured by means of a one-dimensional (1D) numerical model. Despite the rapid evolution of computational power, 1D models are required for the prediction of long-term and large scale river processes.

Since the seminal models of Engelund ([18]) and Ikeda, Parker and Sawai ([19]), mathematical models of meander hydrodynamics and meander migration have been continuously further developed and refined. Recent developments were mainly made by Seminara ([20]), Camporeale et al. ([21]), Crosato (chapter 4, [22]) and Pittaluga et al. ([23]). The latter summarizes and compares existing 1D models for meander migration. All of these models are somehow based on the assumption of mild curvature. Blanckaert and de Vriend ([24], [25]) have proposed a 1D model for meander hydrodynamics that remains valid in the high curvature range and encompasses the mild-curvature model of Johannesson and Parker ([26]). Their model can formally be written in the form of a linear relaxation equation in the variable α_s that parameterizes the transverse distribution of the streamwise velocity, with adaptation length $\lambda_{\alpha s}/R$ and driving mechanism $F_{\alpha s}/R$:

$$\frac{\alpha_s}{R} = (1 + n/R)\frac{1}{U_s}\frac{\partial U_s}{\partial n} \tag{2}$$

$$\lambda_{\alpha s/R}\frac{\partial}{\partial s}\left(\frac{\alpha_s}{R}\right) + \frac{\alpha_s}{R} = F_{\alpha s/R} \tag{3}$$

$$\lambda_{\alpha s/R} = \frac{1}{2}\frac{H}{\psi C_f}\left\{1 - \frac{1}{12}\frac{\alpha_s + 1}{R}\frac{B^2}{R}\right\} \tag{4}$$

$$\begin{aligned} F_{\alpha s/R} = {} & \frac{1}{2}\frac{S_n Fr^2 + \mathrm{A} - 1}{R} \\ & - \frac{1}{2}\frac{H}{\psi C_f}\frac{\partial}{\partial s}\left(\frac{1}{R}\right)\left(1 - \frac{B^2}{6R^2}\right) \\ & + \frac{4\chi}{\psi C_f}\frac{H^2}{B^2}\frac{\langle f_s f_n\rangle}{R}\left[1 + \frac{1}{12}\frac{(S_n Fr^2 + \mathrm{A} + 3)B^2}{R^2}\right] \\ & + \frac{1}{24}\frac{H}{\psi C_f}\frac{B^2}{R^2}\frac{\partial}{\partial s}\left(\frac{S_n Fr^2 + \mathrm{A}}{R}\right) \end{aligned} \tag{5}$$

The coefficient ψ parameterizes curvature-induced energy losses and S_n is a coefficient of order 1. This equation clearly indicates the processes underlying the velocity redistribution. The first term (I) in Equation (5) represents the effect of the transverse slopes of the bed and the water surface, parameterized by the coefficient A and the Froude number, respectively. The second term (II) represents local flow accelerations/decelerations due to the adaption of the transverse water surface slope (superelevation) to changes in curvature. The third term (III) represents velocity redistribution by the secondary flow. It is parameterized by $\langle f_s f_n\rangle / R$, which is determined from the relation (see [24]):

$$\langle f_s f_n\rangle = fct(C_f)\, fct\left(C_f^{-0.275}\left(\frac{H}{R}\right)^{0.5}(\alpha_s + 1)^{0.25}\right) \tag{6}$$

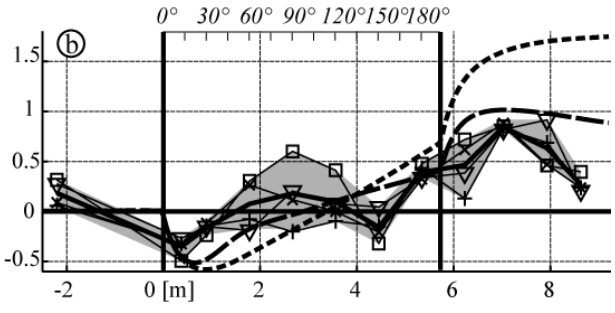

Figure 8: Evolution of α_s/R around the flume in the mobile-bed experiment obtained from: (i) the experimental data (labeled lines, full lines and gray area) (ii) the proposed 1D model without curvature restrictions (long-dashed line); (iii) the proposed model in its asymptotic formulation for mild curvature (short-dashed line).

The second functional relation in Equation (6) accounts for the non-linear interaction between the horizontal flow distribution (α_s) and the vertical flow distribution ($f_s f_n$). The fourth term (IV) represents velocity redistribution by the cross-flow U_n resulting from streamwise variations in the transverse slopes of the bed and the water surface. When assuming that B/R is small, $\psi \approx 1$, the coefficient χ=1.5, and the second functional relation in Equation (6) is identical to one, the model reduces to the widely used mild-curvature model of Johannesson and Parker ([26]).

Figure 8 compares the evolution of α_s /R around the bend in the laboratory experiment, obtained from: (i) the experimental data; (ii) Blanckaert and de Vriend's 1D model without curvature restrictions; (iii) Blanckaert and de Vriend's 1D model in its asymptotic formulation for mild curvature. Obviously the complex 3D velocity pattern can only be parameterized by means of the single variable α_s /R (cf. Equation (2)) in an approximate way. Therefore, Figure 8 includes an uncertainty range (gray area) for the estimations from the experimental data. The mild curvature model significantly overestimates the outwards velocity distribution. Although significant deviations occur locally, the proposed model without curvature restrictions agrees globally satisfactorily with the data. Obviously a depth-integrated and width-integrated 1D description can only account for processes that occur on a spatial scale of the order of magnitude of the river width. The description of processes on a smaller spatial scale requires a 2D or 3D description and modeling approach. The resolution of the 1D approach is coherent, however, with the objective of investigating long-term and large scale river planform processes.

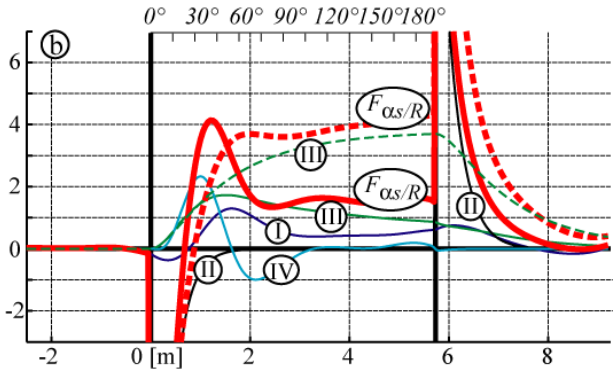

Figure 9: Evolution around the flume of the mechanisms that drive the velocity redistribution according to Equation (5) for the model without curvature restrictions (full lines) and the mild-curvature model (dashed lines). The labels on the curves correspond to the terms in Equation (5).

The transparency of the 1D model is exploited in Figure 9, which shows the evolution around the bend of the mechanism that drive the velocity redistribution according to Equation (5). According to the model, all four mechanisms are of dominant order of magnitude. Remarkably, variations in curvature (term II) are the dominant contribution. Differences between the model without curvature restrictions and the mild-curvature model are considerable and include: (i) a reduction of the effect of the secondary flow (term III) due to non-linear interactions between the horizontal and vertical structures of the flow; (ii) velocity redistribution due to streamwise changes in the bed and water surface topography (term IV) which are not accounted for in the mild-curvature model; (iii) reduction of the driving mechanisms due to the curvature-induced increase in energy losses parameterized by ψ (Terms II, III and IV).

More in general, the proposed model identifies $C_f^{-1}H/R$ as the main control parameter with respect to the velocity redistribution in curved open-channel flow. The driving mechanisms related to streamwise variations in curvature and the transverse bed and water surface slopes scale with it and the normalized adaptation length, λ_{cs}/R (cf. Equation (4)) is proportional to it. de Vriend ([27]) identified $C_f^{-1}H/R$ as an important control parameter. Because it represents a ratio between forcing by curvature (H/R) and dissipation by boundary-friction generated turbulence (C_f), he called $C_f^{-1}H/R$ the Dean number, similar to its definition in curved laminar flow. Blanckaert and de Vriend ([24]) identified $C_f^{-1}H/R$ as a major control parameter with respect to the vertical structure of the flow field and its interaction with the transverse flow structure. Johannesson and Parker ([26]) identified a similar parameter, $2\pi C_f^{-1}H/\lambda_m$ λ_m is the meander wavelength which they called the reduced wavenumber. The ratio B/R is traditionally the major scaling parameter used in field studies on meandering rivers. With respect to the velocity redistribution, B/R does not play a major role in mildly curved bends, but may be significant in sharp bends (cf. Equations (5)). The parameter set $C_f^{-1}H/B$ and B/R is equivalent to the parameter set $C_f^{-1}H/R$ and B/R. $C_f^{-1}H/B$ has the advantage that it characterizes a river reach and is independent of the curvature of individual bends.

The hydrodynamic model without curvature restrictions ([24], [25]) has been validated by means of the here reported laboratory experiment, which constitutes an extremely demanding case due to its very sharp curvature and its very pronounced variations in curvature. The model constitutes a powerful tool to investigate the hydrodynamics in meandering rivers as well as its relation to meander migration. Ottevanger et al. ([28]) have further validated this model by means of field measurements and they have applied it to investigate the processes responsible for the velocity redistribution in various natural meander bends.

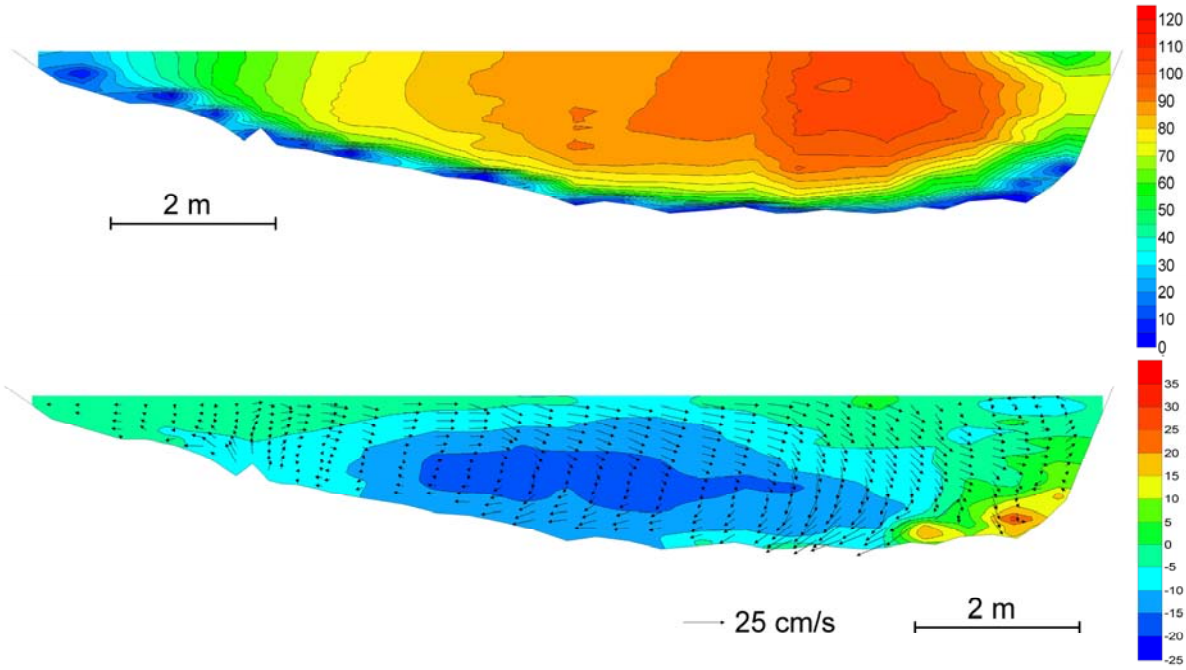

Figure 10: Patterns measured in the S10 cross-section (cf. Figures 4,5) on the Ledra meander bend: (top) Isoline pattern of the streamwise velocity, quantified by the colorbar in [cms^{-1}]; (bottom) Vector pattern of secondary flow and isoline pattern of the transverse-vertical shear stress, quantified by the colorbar in [cm^{2}s^{-2}].

4. The flow field near the bank and its relation to bank erosion processes

According to Equation (1), large-scale and long-term river planform processes are largely driven by the global distribution of the velocity. Understanding river processes on shorter time scale and a smaller spatial scale requires more detailed knowledge of the flow field. Bank erosion processes on the time-scale of a flood event and on a local spatial scale, for example, depend on the geotechnical behavior, the flow field near the bank and its interaction with groundwater flow.

Equation (1) does not account for the complex near-bank hydrodynamics, such as additional cells of secondary flow near the bank (e.g. [29], [30], [31], [32], [33], [34], [35], [36], [37]) or the flow separation and recirculation at the convex banks ([38], [39], [40]) or the formation of benches at concave banks accompanied by flow recirculation ([41], [42], [43], [44]). This section will focus on the flow pattern near the outer bank in meander bends.

Figure 10 illustrates patterns of the 3D flow field measured in the cross-section S10 of the Ledra meander bend (cf. Figures 4, 5). Streamwise velocities are rather low over the shallow inner part of the cross-section, but characterized by a considerable transverse gradient. The velocities increase in outwards direction, but the core of maximum velocities stays at about 2m, corresponding to about once the local flow depth, from the outer bank. Vertical profiles of the velocities are rather flat in this region, and characterized by important near-bed gradients and a maximum value that occurs slightly below the water surface. The secondary flow, defined as the projection of the velocity vector in the cross-section, shows inwards mass transport over the entire flow depth close to the inner bank over the shallowest par of the cross-section. The typical curvature-induced secondary flow occurs in the central part of the cross-section.

The most important feature with respect to bank erosion processes is the occurrence of a counter-rotating outer-bank cell of secondary flow in the upper part of the flow depth adjacent to the outer bank. It occupies a zone with a width of about once the local flow depth. The core of maximum streamwise velocities seems to coincide with the separation between both secondary flow cells. In the same region, advection of flow towards the toe of the outer bank occurs, but it does not result in a discernable increase of near-toe streamwise velocities. The pattern of both secondary flow cells is very well reflected in the pattern of cross-sectional (transverse-vertical) shear stress.

As aforementioned, vegetation, outer-bank benches and local bank erosion created an irregular geometry of Ledra's banks, which complicates the analysis of the near-bank flow patterns and the outer-bank cell of secondary flow. The influence of the inclination and

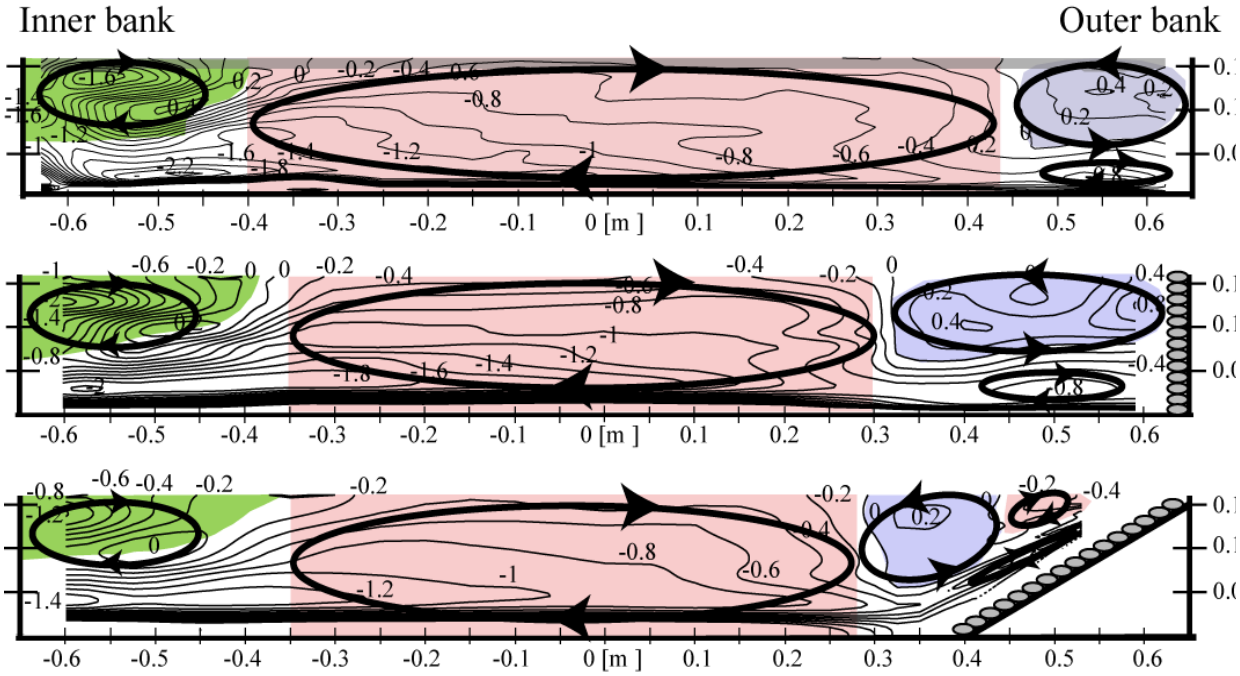

Figure 11: Measured patterns of the secondary flow, quantified by the normalized streamwise component of the vorticity, $\omega_x H/U$ in experiments with fixed horizontal bed and smooth vertical outer bank (top), riprap-roughened vertical outer bank (middle) and riprap-roughened outer bank inclined at 30° (bottom).

roughness of the outer bank has therefore been investigated in a series of nine experiments in the laboratory flume shown in Figure 6. The bed was horizontal and consisted of immobilized sand. Three different bank inclinations (30°, 45° and 90°) and three different roughness characteristics (smooth, the same sand roughness as the bed and riprap with a equivalent roughness of k_s = 30 mm) were investigated by Duarte ([45]). The experiments were carried out with similar overall flow depth of H = 0.16m and overall velocity of U = 0.43 ms^{-1}.

The outer-bank cells are known to be relevant with respect to the stability of the outer bank and the adjacent bed. According to Bathurst, Thorne and Hey ([32]) they endanger bank stability, whereas Blanckaert and Graf ([46]) found that they protect the outer bank and the adjacent bed by forming a buffer layer that protects the outer bank and adjacent bed from any influence of the center-region cell: the central secondary flow cell redistributes the velocity and causes it to increase towards the outer bank, whereas the outer-bank cell prevents this increase to continue through to the bank and keeps the core of maximum velocity a distance from the bank at the separation between both cells. The measurements in the Ledra comply with Blanckaert and Graf's ([46]) results.

Figure 11 illustrates the measured patterns of the secondary flow in the cross-section at 90° in the bend in experiments with smooth vertical outer bank, rough vertical outer bank, and rough 30°-inclined vertical outer bank. The secondary flow is quantified by means of the streamwise component of the vorticity, defined as $\omega_s = \partial v_z/\partial n - \partial v_n/\partial z$. Outer-bank cells occurred in all nine investigated conditions. An increase in outer-bank roughness widens and strengthens considerably the outer-bank cell, whereas inclining the outer bank weakens the outer-bank cell and changes its pattern. But its protective effect by forming a buffer layer between the outer bank and the center-region cell is conserved. More details are reported in Duarte ([45]).

Blanckaert and de Vriend ([4]) have analyzed the mechanisms underlying the near-bank secondary flow cells by means of a term-by-term analysis of the vorticity equation and the kinetic energy fluxes between the mean flow and the turbulence. Based on their results they have postulated that the outer-bank cell can only be resolved by turbulence models that can account for the backscatter of kinetic energy from the turbulence to the mean flow. This hypothesis was confirmed in numerical simulations by van Balen et al. ([47]), who accurately resolved the outer-bank cell in the reported laboratory experiments with horizontal bed and smooth vertical banks (cf. Figure 11) by means of a Large Eddy Simulation (LES) numerical model, but did not succeed to resolve them by means of a Reynolds Averaged Navier Stokes (RANS) model with two-equation turbulence closure (see Figure 12).

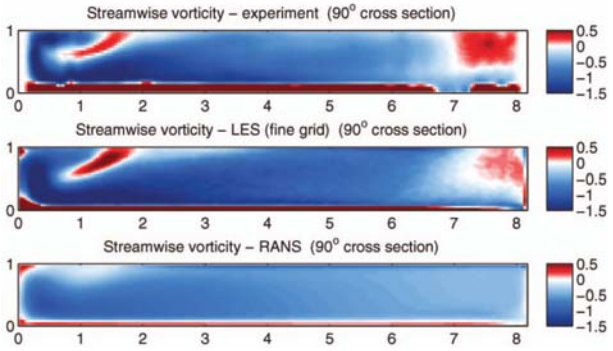

Figure 12: Patterns of the secondary flow, quantified by $\omega_s H/U$ in the experiment with fixed horizontal bed and smooth vertical banks. (top) Experimental data, (middle) LES simulation, (bottom) RANS simulation. Figure modified from ([47]).

The results from the validated numerical LES model allow gaining further insight in the meander hydrodynamics. Contrary to the experimental data, the simulated data are not limited by a low spatial resolution in streamwise direction or by experimental scatter and uncertainty. Hence they are particularly appropriate for term-by-term analyses of the flow equations. Van Balen et al. ([47]) have analyzed the mechanisms underlying the near-bank cells of secondary flow and highlighted the important role played by turbulence. The LES simulations also provide data in flow regions that are not accessible by the velocimeters, such as the flow regions close to the solid boundaries and the water surface, and variables that cannot easily be measured, such as the pressure distribution or the boundary shear stress. The letter plays a dominant role with respect to morphodynamical processes, and especially with respect to bank erosion processes. The distribution of the shear stress on the outer bank, shown in Figure 13, is clearly affected by the outer-bank cell of secondary flow. A more detailed description can be found in Van Balen et al. ([48]). The validated LES code also allows a broadening of the parameter space in order to obtain generic results on the bank shear stress that are valid for a wide range of natural rivers.

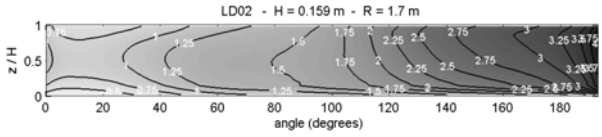

Figure 13: Patterns of the normalized shear stress on the outer bank, $\tau_{bank}/\rho U^2$ in the experiment with fixed horizontal bed and smooth vertical banks obtained from LES simulations. Figure modified from ([48]).

5. Invertebrate dynamics and their relation to the flow field and the turbulence

Understanding invertebrate assemblages' dynamics in relation to flow dynamics, morphodynamic and sedimentological processes is a key approach in understanding river ecological functioning. Changes in flow dynamics have direct consequences on invertebrate individuals, i.e. drift (Gibbins et al. ([49]), Gabel et al. ([50])) or changes in prey-predator relationships (Hart and Finelli ([51]), Gabel et al. ([52])). Flow dynamics also influence habitat structure and food resource availability, two main components shaping invertebrate assemblages. For example, increases in flow velocities will trigger erosive processes, removing local silt deposits and organic debris as well as fine sand particles. The physical habitat for invertebrates switches then from fine instable organic enriched substrate to coarse more stable organic-poor substrate. As a result, invertebrate assemblages will change from communities dominated by sediment eaters or collector-gatherer taxa to communities dominated by filterer taxa.

This mechanism is however more complicated since each taxa has a range of tolerance to changes in environmental conditions, allowing a certain resilience of the communities in the ecosystem. Flow variations also differently influence environmental conditions at local scale according to local geomorphology or the presence of macrophytes. Hence, far to be simple and linear, the influence of flow dynamics on invertebrates is complicated by the dense network of interactions linking all components of the river ecosystem at different spatial and temporal scales.

Our ongoing research links field scales, laboratory and numerical approaches to examine the linkages between complex flow, morphology and ecology in meander bends, and especially their effect on aquatic invertebrate distributions and the use of food resources. Questions of interest that are addressed include:

- How and to what extend, daily and seasonal natural changes in hydrodynamic conditions influence the density of benthic invertebrates?
- What are the hydrodynamic parameters of relevance with respect to the drift of invertebrates?
- Do revitalized rivers provide better ecological conditions for invertebrates and how can this be quantified?

The field investigation was designed to describe and quantify benthic invertebrate assemblages, habitat structure and food availability at representative locations in meanders, in strict correspondence to local hydraulic conditions. The survey was performed along riffle and pool transects (Figure 14). A detailed description and quantification of the habitat structure (size fraction of the upper 5 cm of sediment, macrophytes mapping, and record of the presence of hard - stones or coarse woody-debris substrates) as well as food availability (thickness and organic fraction of silt cover, biofilm and seston concentrations) was done on a 2m x 2m grid at each transect (Figure 14). Benthic invertebrates were collected at all differing meso-habitats - as characterized by a combination of specific flow and habitat conditions - identified at the date of the survey.

In order to link ecological parameters and hydraulics conditions, each sampling location was geographically referenced in the geographical system set up to establish topography and flow fields of the bend, and water level was recorded at referenced gauging stations installed upstream and downstream the meander. The survey was performed 4 times a year in order to count for seasonal differences in invertebrate assemblages.

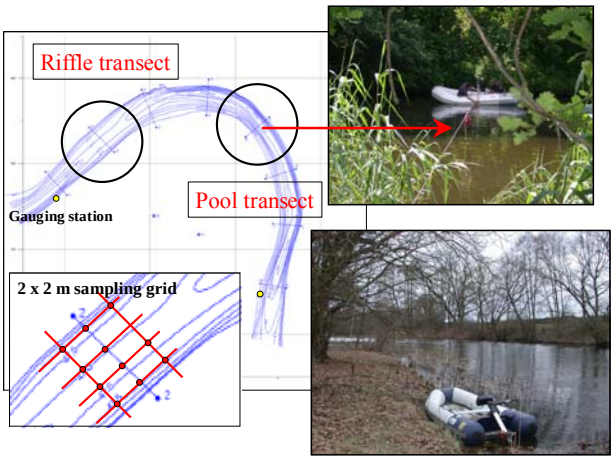

Figure 14: Illustration of the field sampling strategy used to survey benthic assemblages, habitat structure and food availability in strict correspondence to hydraulic characteristics on the Spree River meander at Neuenbrück, NE Germany. The top picture shows the marked cable used to reference geographically each sampling location.

Invertebrates were collected using a Surber net sampler of 250 µm mesh size and 0.05 m² sampling surface (Figure 15) operated under water by direct diving. A metal stick, positioned from a boat at the desired sampling location along the transect served as guide to locate the exact sampling location when diving. Once the Surber sampler in place on the river bottom, the upper 5 centimeter of sediment (or any other sampled substrates, i.e macrophytes, stones, dead wood) are pushed into the net where they stay trapped by the flow. Back at the surface, the samples are fixed with 70% ethanol. Invertebrates colonizing hard substrates were detached by gently scratching the collected pieces with a brush (Figure 15). The scratched surface areas were recorded in order to calculate densities. At the laboratory, invertebrates were separated from the substrate, counted and identified till species level under stereo-microscope (Figure 16).

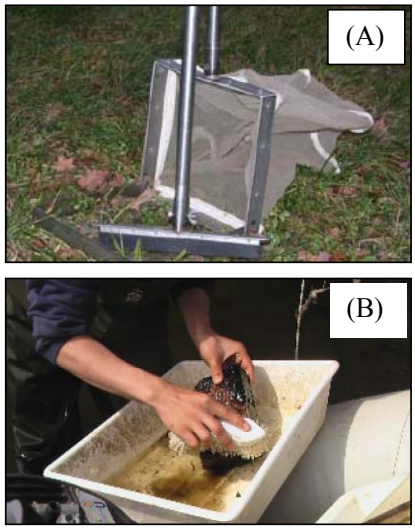

Figure 15: Surber net device (A) and brushing technique (B) used to collect benthic invertebrates.

Beside recording invertebrate densities for various flow conditions, identifying the origin of food ingested by the individuals of each taxa for these various flow conditions is of key importance aspect. For that purpose we used the stable isotope analysis approach. Conceptually, each food resource exhibits a specific ratio of C13/N15 isotopes which stays unchanged in invertebrate tissues when individuals mainly feed on that food resource. δN15 values increase through trophic levels but δC13 values do not change. Hence, it becomes easy to link food availability with the trophic regime of benthic individuals. Moreover, by correlating this information to quantitative information on food distribution, it becomes possible to estimate at what thresholds changes in food resources trigger changes in invertebrate assemblages.

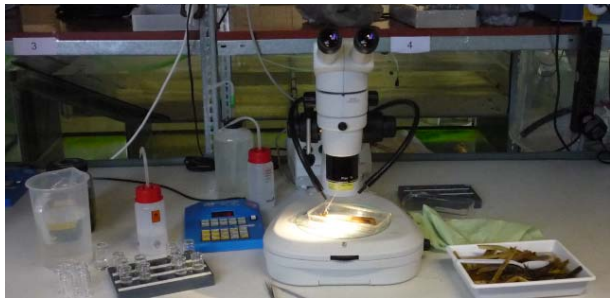

Figure 16. Typical working station to process invertebrate samples in the laboratory.

Figure 17 illustrates possible mechanisms of shift in community composition due to changes in flow condition. The two graphs represent the food-web situation at two locations on the River Mulde (North-east Germany) that have different flow characteristics: plot A concerns high flow velocities (0.72 $m.s^{-1}$) whereas plot B concerns low flow velocities (0.23 $m.s^{-1}$). The sediment structure was comparable at the two locations, with the exception of the presence of a slightly thicker silt cover in location B due to lower flow velocities. Isotope analysis shows that communities of filterer taxa characterized by *Hydropsychae contubernalis*, *H. pelucidulla*, *Pisidium* sp (Figure 18) and *Sphaerium* sp dominate at high flow velocities. These taxa feed on seston transported through the water column as shown by the comparable values of δ13C found in the seston and the body tissues of these species.

At low flows, obligatory filterers like *Pisidium* sp or *Sphaerium* sp have disappeared. Collector gatherer taxa like *Caenis* sp, *Limoniidae* or *Tipulidae* (Figure 19), collecting fine deposited organic particles dominate the assemblages. The case of the *Tipulidae* is especially illustrative. The individuals of this taxa directly feed on the fine particulate organic material (FPOM) deposited at

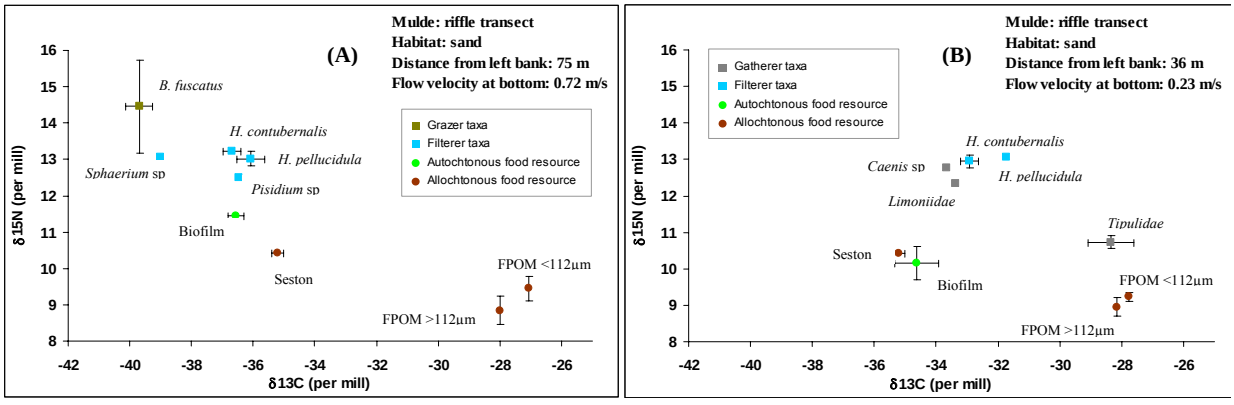

Figure 17: Plots of δ13C/δ15C ratios for benthic invertebrates and food resources collected in sand habitat at high (A) and low (B) flow velocities, respectively. FPOM: Fine Particulate Organic Matter.

the surface of the sand as shown by the comparable values of δ13C found in the FPOM and the body tissues. *Caenis* sp and *Limoniidae* individuals probably feed more on the organic particles deposited or trapped in the biofilm. It is also interesting to see that non-obligatory filterer like *H. contubernalis* and *H. pellucidula* shift for a food regime more composed of deposited organic material as suggested by the shift, of 4 units of δ13C towards characteristic values for FPOM in their body tissue.

Hence, it is easy to imagine that a drop in flow velocity on location A will favor the presence of the collector gatherer taxa, similarly to location B. Conversely, increasing flow at location B will favor the colonization of sand by true filter taxa like *Pisidium* sp or *Sphaerium* sp. This result exhibit how hydrodynamics trigger modification of invertebrate assemblages by controlling food availability.

Species distributions, however, do not only depend on such processes, but also on direct drag forces exerted by the flow on species individuals, and on how species with different body form and gripping strategies cope with these forces (see Gabel et al. ([50]), Schnauder et al. 2010 ([53])). Where the study of the links between food and species distribution typically requires field investigations, the quantification of thresholds in drag forces for drifting species individuals and the study of the ongoing processes in invertebrate drift can be investigated under controlled laboratory conditions. Both approaches are complementary to achieve a realistic model of species distribution according to flow dynamics.

Figure 18. Specimen of *Pisidium* sp, a typical filterer taxa

Figure 19. Specimen of *Tipulidae*, a typical collector-gatherer taxa

In orer to investigate the hydrodynamic parameters, and especially the role of turbulence, implicated in invertebrate drift, a set of experiments was performed that expose three benthic invertebrate taxa (*Aeshna cyanea*, *Calopteryx splendens* and *Cordulia* sp.) to three different levels of turbulence intensity. Each test was replicated three times, resulting in a set of 27 experimental cases. The experiments were performed in a laboratory flume that represents an alpine confluence. The bed topography and sedimentology in the main channel are the result of the interplay between flow and sediment transport, leading to pronounced transverse bed slopes and sediment sorting. Invertebrates were successively exposed to flow at locations differing in turbulence levels. The lowest level of turbulence was obtained upstream of the confluence where the flow is quasi-uniform. A higher turbulence level was found in the confluence zone due to the inclined bed topography and the coarser sediments, even without discharge in the tributary. The turbulence level was further increased due to 3D flow effects when the tributary contributed to the discharge. For each test, the discharge was increased until invertebrate drift occurred

The investigation required the use of state-of-the art experimental techniques. The turbulent velocity fields in the vicinity of the invertebrate were measured by means of the Acoustic Doppler Velocity Profiler (ADVP, cf. section 2). The ADVP's profiling capacity and its flexibility to follow the moving invertebrates were essential in this investigation. Simultaneously, the invertebrate behavior was recorded using a high acquisition rate video camera operated at 5 Hz. This allowed determining accurately the drift moment.

Figure 20 illustrates the results for an experiment carried out with the invertebrate species "*Aeshna cyanea*". ADVP measurements provided with a temporal resolution of 31.25 Hz the velocity field in the vertical profile located above the invertebrate. The Taylor hypothesis of frozen turbulence allows converting the temporal series into a spatial pattern of turbulent structures in the vertical plane that containing the invertebrate and that is oriented along the flow direction (Figure 20(d)). These preliminary experiments suggest that invertebrate drift is related to turbulence events. Figure 20(d), for example, shows considerable turbulent accelerations near the invertebrate at the drift moment.

The objective of this research is to implement the new knowledge in a numerical model that accounts for the linkages between invertebrate dynamics, the hydrodynamics, the sediment transport and the morphodynamics. Such a tool would allow a better evaluation of the ecological value of rivers and a quantification of the gain obtained in river revitalization projects.

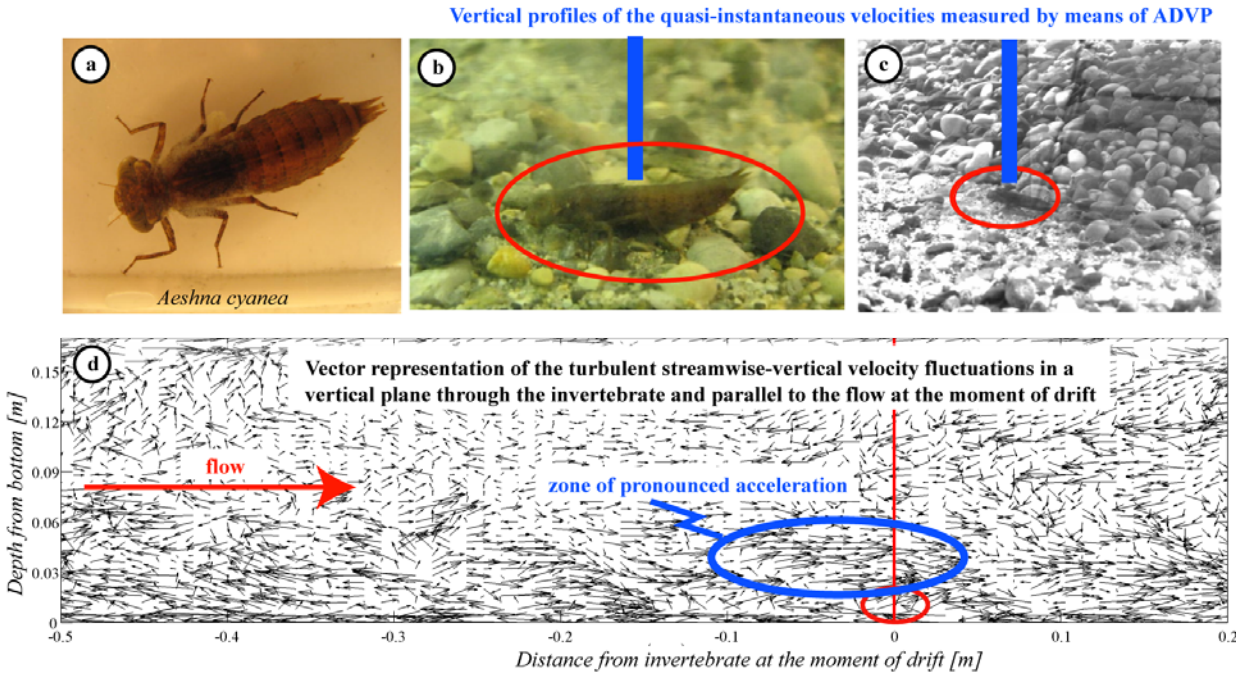

Figure 20: (a) One of the invertebrate species investigated, (b), (c) Close-up of the invertebrate sitting on the gravel bed in the flume with indication of the vertical flow profiles measured above the invertebrate, (d) Vector representation of the turbulent streamwise-vertical velocity fluctuations in a vertical plane through the invertebrate and parallel to the flow at the moment of drift.

6. Conclusions

Hydrodynamical, morphodynamical and ecological river processes and their multiple linkages occur in an infinity of different configurations and over a wide range of spatial and temporal scales. This paper has illustrated a research methodology that consists in combining field investigations, physical modeling in the laboratory, and numerical simulations in order to develop generic insight and tools for engineering and management of the river environment.

The first illustration of this methodology concerned the investigation of the velocity distribution in meander bends, which is known to be a predominant forcing mechanism for the long-term and large-scale planimetric evolution of meanders. Detailed velocity measurements performed in a natural meander bend were presented. They revealed the dominant hydrodynamic processes, but their interpretation and analysis were hindered by the presence of floating wood, vegetation, outer-bank benches and local bank erosion. These dominant processes were subsequently investigated under controlled conditions in a physical model in the laboratory. Based on the analysis of the laboratory investigation, a numerical model for the velocity redistribution was developed, which computational requirements allow its application on a large spatial scale and/or a long temporal scale.

The second illustration concerned the investigation of the hydrodynamics near the river bank, which are relevant for bank erosion processes on the time-scale of a flood event and on a local spatial scale. Field investigations in a meander bend revealed that the near-bank hydrodynamics are conditioned by the existence of a so-called outer-bank cell of secondary flow. This outer-bank cell of secondary flow was subsequently investigated under controlled laboratory conditions. Attention was focused on its dependence on the roughness and inclination of the outer bank. Based on the insight provided by the laboratory experiments, requirements for the numerical simulation of the outer-bank cell were defined, resulting in the successful simulation of the near-bank hydrodynamics by means of a three-dimensional Large Eddy Simulation model. This model provided the shear stress on the outer bank. This is the most important parameter with respect to the flow attack on the bank, but it could not directly be obtained from the laboratory experiments.

The third illustration concerned the investigation of the linkages between three-dimensional flow patterns, turbulence, morphology and ecology in meander bends. Field measurements were performed that mapped the local hydraulic and morphologic conditions, the habitat structure of invertebrates and the availability of food

resources. Complementary laboratory experiments investigated thresholds in mean drag forces and turbulent coherent structures for drifting species individuals, and on how species with different body form and gripping strategies cope with these forces. The insight provided by the field and laboratory investigations will be implemented in a numerical model that accounts for the linkages between invertebrate dynamics, the hydrodynamics, the sediment transport and the morphodynamics.

Acknowledgments

This research was sponsored by the Swiss National Science Foundation under grants 2100-052257, 2000-059392. 2100-066992, 20020-103932 and 200020-119835, by the Deutsche Forschungsgemeinschaft (DFG) and the Netherlands Organization for Scientific Research (NWO) under grants SU 405/3-1 and DN66-149 in the framework of their bilateral cooperation program. The first author was partially funded by the Chinese Academy of Sciences fellowship for young international scientists under Grant No. 2009YA1-2.

References

[1] Lemmin, U., and Rolland, T. (1997). ‘‘Acoustic velocity profiler for laboratory and field studies.’’ *J. Hydraul. Eng*., 123(12), 1089–1098.

[2] Hurther, D., and Lemmin, U. (1998). ‘‘A constant beamwidth transducer for three-dimensional Doppler profile measurements in open channel flow.’’ *Measurement Science and Technology*, 9(10), 1706–1714.

[3] Blanckaert, K., and Graf, W. H. (2001). “Experiments on flow in an open-channel bend. Mean flow and turbulence.” *J. Hydraul. Eng*.,127(10), 835–847.

[4] Blanckaert, K., and de Vriend, H. J. (2004). “Secondary flow in sharp open-channel bends.” J. Fluid Mech., 498, 353–380.

[5] Blanckaert, K., and Lemmin, U. (2006). “Means of noise reduction in acoustic turbulence measurements.” *J. Hydraul. Res*., 44(1), 3–17.

[6] Blanckaert, K. (2010) “Topographic steering, flow recirculation, velocity redistribution and bed topography in sharp meander bends”, *Water Resour. Res*., doi:10.1029/2009WR008303, in press

[7] Pizzuto, J., and T. Meckelnburg (1989). “Evaluation of a linear bank erosion equation”. *Water Resour. Res*., 25, 1005–1013.

[8] Whiting, P. J., and Dietrich, W. E. (1993). “Experimental studies of bed topography and flow patterns in large-amplitude meanders. I: Observations.” *Water Resour. Res*., 29 11 , 3605–3614.

[9] Abad, J. D., and M. H. Garcia (2009), Experiments in a high-amplitude Kinoshita meandering channel: 2. Implications of bend orientation on bed morphodynamics, *Water Resour. Res.*, 45, W02402, doi:10.1029/2008WR007017.

[10] Yen C. and B.C. Yen BC (1971). “Water surface configuration in channel bends”. *J. Hydraul. Div.*., 97(HY2), 303-321.

[11] de Vriend, H.J. and Koch, F.G. (1978). “Flow of water in a curved open channel with a fixed uneven bed”. T.O.W. Rep. R657-VI/M1415-II, Delft Hydraulics Lab., Delft Univ. Techn., The Netherlands.

[12] Hooke, R. L. (1974), Shear-stress and sediment distribution in a meander bend, Tech. Rep. UNGI RAPPORT 30, Dep. of Phys. Geogr., Univ. of Uppsala, Uppsala, Sweden.

[13] Kikkawa H, Ikeda S and Kitagawa A. (1976). “Flow and bed topography in curved open channles”. *J. Hydraul. Div*., 102(9), 1327-1342.

[14] Odgaard, A. J., and Bergs, M. A. (1988). ‘‘Flow processes in a curved alluvial channel.’’ *Water Resour. Res*., 24(1), 45–56.

[15] Leeder, M. R. and Bridge, P.H. (1975). "Flow separation in meander bends". *Nature*, 253, 338– 339, 1975.

[16] Frothingham, K.M. and Rhoads, B.L. (2003). “Three-dimensional flow structure and channel change in an asymmetrical compound meander loop, Embarras River, Illinois”. *Earth Surface Processes and Landforms*, 28(6), 625-644.

[17] Ferguson, R.I., Parsons, D.R., Lane, S.N. and Hardy, R.J. (2003). "Flow in meander bends with recirculation at the inner bank". *Water Resour. Res*. 39(11): 1322.

[18] Engelund F. (1974). “Flow and bed topography in channel bends”. *J. Hydraul. Div*., 100(HY11), 1631-1648.

[19] Ikeda, S., Parker, G., and Sawai, K. (1981). “Bend theory of river meanders. Part 1. Linear development.” *J. Fluid Mech*., 112, 363-377.

[20] Seminara G. (2006). “Meanders”. *J. fluid mech.*, 554, 271-297.

[21] Camporeale, C., P. Perona, A. Porporato, and L. Rodolfi (2007), Hierarchy of models for meandering rivers and related morphodynamic processes, *Rev. Geophys*., 45, RG1001, doi:10.1029/2005RG000185.

[22] Crosato A. (2008). “Analysis and modelling of river meandering”. PhD thesis, Delft University of Technolgy, Delft, The Netherlands

[23] Pittaluga M.B., Nobile G. and Seminara G. (2009). “A nonlinear model for river meandering”. *Water Resour. Res*. 45, Article Number: W04432.

[24] Blanckaert, K., and de Vriend, H. J. (2003). “Nonlinear modeling of mean flow redistribution in curved open channels.” *Water Resour. Res.*, 39(12), 1375–1388.

[25] Blanckaert K. and de Vriend H.J. (2010). “Meander dynamics: a nonlinear model without curvature

restrictions for flow in open-channel bends". *J. Geoph. Res*., doi: 10.1029/2009JF001301, in press.
[26] Johannesson, H. and Parker, G. (1989). "Velocity redistribution in meandering rivers." *J. Hydraul. Eng*., 115(8), 1019-1039.
[27] de Vriend, H. J. (1981). "Velocity redistribution in curved rectangular channels." *J. Fluid Mech*, 107, 423-43
[28] Ottevanger W., Blanckaert K. and UittewaalW.S.J. "Analysis of the mechanisms responsible for streamwise velocity redistribution in natural rivers ». *Geomorphology*. (submitted for publication).
[29] Hey, R.D. and Thorne, C.R. (1975). "Secondary flow in river channels". *Area*, 7(3), 191-195.
[30] Bridge, J.S. and Jarvis, J. 1977. "Velocity profiles and bed shear stress over various bed configurations in a river bend". *Earth Surface Proc*., 2, 281-294.
[31] Bathurst, J. C., Thorne, C. R., and Hey, R. D. (1977). "Direct measurements of secondary currents in river bends." *Nature*, 269, 504-506.
[32] Bathurst, J. C., Thorne, C. R. and Hey, R. D. (1979). "Secondary flow and shear stress at river bends." *J. Hydr. Div.* 105(10), 1277-1295.
[33] Thorne, C. R., and Hey, R. D. (1979). "Direct measurements of secondary currents at a river inflexion point." *Nature*, 280, 226-228.
[34] Dietrich, W. E., and J. D. Smith (1983). "Influence of the point bar on flow through curved channels". *Water Resour. Res.*, 19(5), 1173– 1192.
[35] de Vriend, H. J. & Geldof, H. J. (1983). "Main flow velocity in short and sharply curved river bends". Rep. 83-6, Lab. Fluid Mech., Dept. Civil Engng, Delft University of Technology.
[36] Thome, C.R., Abt, S.R., and Maynord, S.T. (1995). "Prediction of near-bank velocity and scour depth in meander bends for design of riprap revetments". In: River, coastal and shoreline protection; Erosion control using riprap and armourstone, Eds. C.R. Thorne, S.R. Abt, F.B.J. Barends, ST., Maynord and K.W. Pilarczyk, Wiley, pp. 115-133.
[37] Markham, A. J., and Thorne, C. R. (1992). "Geomorphology of gravel-bed river bends." Dynamics of gravel-bed rivers, P. Billi, Hey, R.D., Thorne, C.R. and Tacconi, P., ed., Wiley, 433-456.
[38] Leeder, M. R., and Bridges, P. H. (1975). "Flow separation in meander bends." *Nature*, 253(5490), 338-339.
[39] Frothingham, K.M. and Rhoads, B.L. (2003). "Three-dimensional flow structure and channel change in an asymmetrical compound meander loop, Embarras River, Illinois". *Earth Surface Processes and Landforms*, 28(6), 625-644.
[40] Ferguson, R.I., Parsons, D.R., Lane, S.N. and Hardy, R.J. (2003). "Flow in meander bends with recirculation at the inner bank". *Water Resour. Res.*, 39(11): 1322-1333.
[41] Hickin, E. J. (1977). "Hydraulic factors controlling channel migration". In R. E. Davidson - Arnott & W. Nickling (editors), Research into Fluvial Systems, GeoAbstracts, Norwich, 59-66.
[42] Jackson, A.D. (1992). "Bedload transport and sorting in meander bends, Fall River, Rocky Mountain National Park, Colorado". PhD , Colorado State University, Fort Collins, colorada, 280p
[43] Andrle, R. (1994). "Flow structure and development of circular meander pools". *Geomorphology*, 9, 261-270.
[44] Hodskinson, A., and Ferguson, R. I. (1998). "Numerical modelling of separated flow in river bends: Model testing and experimental investigation of geometric controls on the extent of flow separation at the concave bank". *Hydrol. Processes*, 12, 1323–1338, 1998.
[45] Duarte A. (2008). "An experimental study on main flow, secondary flow and turbulence in open-channel bends with emphasis on their interaction with the outer-bank geometry.." PhD-thesis Nr 4227, Ecole Polytechnique Fédérale Lausanne, Switzerland.
[46] Blanckaert, K., and Graf, W. H. (2004). "Momentum transport in sharp open-channel bends." *J. Hydraul. Eng.*, 130(3), 186–198.
[47] Van Balen W, Blanckaert K & Uijttewaal WSJ (2010). "Large-eddy simulations and experiments of single-bend open-channel flow at different water depths". *J. Turbulence*. Vol. 11, Art. No. N 12.
[48] Van Balen W (2010). "Large Eddy Flow Simulation for the prediction of bank erosion and transport processes in river bends" PhD dissertation, Delft University of Technology, The Netherlands.
[49] Gibbins C, Vericat D and Batalla RJ. (2007). "When is stream invertebrate drift catastrophic? The role of hydraulics and sediment transport in initiating drift during flood events". *Freshwater Biology* 52: 2369-2384.
[50] Gabel F, Garcia X.-F, Brauns M, Sukhodolov A, Leszinski M, Pusch MT (2008). "Resistance to ship-induced waves of benthic invertebrates in various littoral habitats". *Freshwater Biology,* 53: 1567-1578
[51] Hart DD, Finelli CM (1999). "Physical-biological coupling in streams: The pervasive effects of flow on benthic organisms". *Annu. Rev. Ecol. Syst.,* 30: 363-395.
[52] Gabel F., Stoll S., Fischer P., Pusch M. and Garcia X.-F. "Waves affect predator-prey interactions between fish and benthic invertebrates". *Oecologia* (Submitted).
[53] I. Schnauder, S. Rudnick, X.-F. Garcia, J. Aberle. (2010). "Incipient motion and drift of benthic invertebrates in boundary shear layers". River Flow proceedings.